Light particle emission induced by stopped antiprotons in nuclei: Energy dissipation and neutron-to-proton ratio

D. Polster, D. Hilscher, and H. Rossner
Hahn-Meitner-Institut Berlin, D-14091 Berlin, Germany

T. von Egidy, F.J. Hartmann, J. Hoffmann, and W. Schmid
Physik Department, Technische Universität München, D-85748 Garching, Germany

I.A. Pshenichnov, A.S. Iljinov, and Ye.S. Golubeva
Institute for Nuclear Research, Russian Academy of Sciences, 117312 Moscow, Russia

H. Machner
Forschungszentrum Jülich, D-52405 Jülich, Germany

H.S. Plendl
Florida State University, Tallahassee, Florida 32306

A. Grochulska, J. Jastrzebski, W. Kurcewicz, and P. Lubinski
Warsaw University, PL-02-097 Warszawa, Poland

J. Eades and S. Neumaier
CERN, CH-1211 Genève 23, Switzerland
(Received 26 September 1994)

Simultaneous measurements of inclusive energy spectra and multiplicities of $\pi^{\pm}$, $K^{\pm}$, n, p, d, and t following antiproton annihilation on nuclei over a wide energy range and in the case of neutrons down to the evaporative part of the spectra are reported. Thirteen targets in the mass range of $A = 12$–238 were used in a target mass dependent investigation of the fast stage of the antiproton-nucleus interaction. The deduced transferred, preequilibrium, and equilibrium excitation energies agree very well with the dynamical picture drawn by the intranuclear cascade (INC) model. Ratios of directly emitted neutrons to protons have been determined to be about twice the N/Z ratio in the target nucleus nearly independently of its mass. These unexpected values for this new sensitive observable are not completely understood in the standard framework of the INC model. Possible effects of isospin and nucleon densities as well as further schemes beyond the INC model are discussed.

PACS number(s): 13.75.Cs, 25.43.+t

I. INTRODUCTION

The physical processes of the production and decay of hot nuclei are of great importance for our understanding of the properties of nuclear matter under extreme conditions. Some of the central questions are, how much energy can a nucleus retain as a self-bound object, at what excitation energies does the nucleus deviate from a sequential statistical decay process, and does a nucleus show phase transitions? These and other questions have been studied in recent years quite extensively [1–3]. Most of these investigations used heavy-ion fusionlike reactions to produce hot nuclei. Though these reactions are quite efficient in heating nuclei they introduce large amounts of rotational and compressional energy [4] into the composite system. In the subsequent decay it is difficult to disentangle effects of angular momentum and compression from the genuine statistical decay of a thermally equilibrated nucleus. Furthermore, fragments produced during the formation phase have to be subtracted in order to obtain the true statistical decay of the hot nuclear system.

That is why one would like to produce hot nuclei with small rotational and compressional energy. The ideal method to achieve this goal would be to use low momentum radiation for which the nucleus represents a black disk. The momentum of this radiation should be small or comparable to the Fermi momentum of about 230 MeV/c of nucleons in nuclei and the mean free path length should be small compared to the nuclear dimension. These conditions are fulfilled by pions with energies close to 195 MeV (or 304 MeV/c) which allow the excitation of a Δ resonance. However, with only one pion of this energy, the maximum energy transfer would be only the kinetic energy plus the mass of the pion, 195+140 =335 MeV. In order to heat the nucleus to higher excitation it would be necessary to irradiate the nucleus simultaneously with several pions; that is, we have to produce several pions close to or even better inside the nucleus. This can be

achieved by the annihilation of antiprotons with a nucleon of the nucleus (see, for instance, [5,6]). The total available energy of 1880 MeV of the annihilation of an antiproton with a nucleon at nearly zero kinetic energy produces an average of five pions ($3\pi^{\pm} + 2\pi^0$) with mean kinetic energies of 210 MeV. The number of pions which will hit the nucleus, which is essentially a black disk for pions, will depend on the proximity of the location of the annihilation process to the nuclear surface. For stopped antiprotons the solid angle of a heavy nucleus with respect to the pion source is about 25% of 4π; that is, on average 1.25 pions will enter the nucleus. This is not very much if one wants to heat the nucleus to high excitation energies, but it is also possible, though with smaller probability, that considerably more pions enter the nucleus. The number of pions hitting the nucleus will drastically increase if the kinetic energy of the antiprotons is increased, in which case the annihilation will take place closer to the center of the nucleus and the pion cloud is focused into the nucleus.

The objective of the present investigation is to test how well we understand the sequence of physical processes after the annihilation of stopped antiprotons in a large variety of target nuclei ranging from ^{12}C to ^{238}U. The model which describes these processes quite well is the intranuclear cascade (INC) model. This model was successful in describing, e.g., the yield of residual nuclei of stopped $\bar{p}$ on Cu [7] and emitted highly energetic p, d, t, ^{3}He, and ^{4}He [8–10].

For $\bar{p}$-induced fission of ^{238}U and ^{209}Bi, Refs. [11,12] investigated the distribution of mass loss $\Delta M = A_T - 1 - A_{F_1} - A_{F_2}$ of a nucleus of mass A_T which fissions into two fragments of mass A_{F_1} and A_{F_2}. The latter work yields information also on the distribution of the thermal excitation energy distribution dissipated within the nucleus.

Only very little data are available for neutron emission after $\bar{p}$ annihilation. Angeloupolos *et al.* [13] measured the high energy component of the neutrons from $\bar{p}$+U, Chen *et al.* [14] the evaporative part of the neutron spectrum of $\bar{p}$+U also, and Minor *et al.* [15] the highly energetic component of the proton spectra. Polster *et al.* [16] measured simultaneously the inclusive n, p, d, t, $K^{\pm}$, and $\pi^{\pm}$ spectra in $\bar{p}$+Cu and U. This work indicated that in particular the neutron-to-proton ratio is unexpectedly large and cannot be reproduced by INC calculations [17,18].

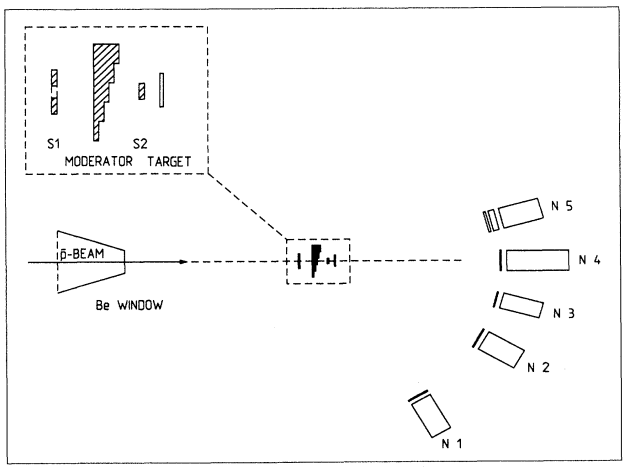

FIG. 1. Schematic setup of the experiment: $N1$–$N5$ particle detectors; the scintillator telescope (S_1,S_2), moderator, and target are shown in the upper left corner (zoomed).

In the present work the measurement of n, p, d, t, $K^{\pm}$, and $\pi^{\pm}$ multiplicities and spectra has been extended to a large range of nuclei from carbon to uranium with special emphasis on the yield ratio of preequilibrium neutrons and protons and the evaporative part of the neutron spectra which is a direct measure of the thermal excitation energy dissipated inside the nucleus.

In Sec. II we briefly describe the experimental setup and the analysis of the data as well as the results. In Sec. III we compare the deduced transfer of energy from the mesonic to the baryonic system. In Sec. IV we discuss the n/p ratio and give in Sec. V a summary of the results.

II. EXPERIMENT

The experiment was carried out as part of PS203 at the low energy antiproton ring (LEAR) at CERN, Geneva. In Fig. 1 the experimental arrangement is schematically shown which was set up completely in air and open geometry. Antiprotons from LEAR with a momentum of 200 MeV/c (equivalent to an energy of about 21 MeV) and an intensity of about (2–5) $\times 10^4$ $\bar{p}$/s passed through a 100 μm thick Be window from vacuum into air and were focused through an annular veto scintillator (inner diameter= 6 mm) $S1$ onto a circular disk scintillator (diameter = 5 mm) $S2$. The thickness of $S2$ was 2.5 mm. The ratio of counting rate in $S1$ to $S2$ was smaller than 1%. About 6–11 mm behind $S2$ the antiprotons were stopped in the center of the following targets: ^{12}C (444), ^{27}Al (270), ^{28}Si (308), ^{nat}Ca (238), ^{nat}Cu (224), ^{92}Mo (207), ^{100}Mo (208), ^{nat}Ag (577), ^{165}Ho (440), ^{181}Ta (830), ^{197}Au (522), ^{209}Bi (784), and ^{238}U (523) where the numbers in parentheses give the thicknesses in mg/cm^2. The range of the antiprotons in the target was adjusted by slowing down the $\bar{p}$ in an energy degrader consisting of Kapton foils and in $S2$. The $\bar{p}$ energies after $S2$ varied between 2.8 and 7.1 MeV. A valid $\bar{p}$ entering into the target was indicated by $\overline{S1} \wedge S2$.

The reaction products induced by stopped $\bar{p}$ in the target were detected with five neutron detectors $N1$, $N2$, $N3$, $N4$, and $N5$ positioned between 141 and 271 cm from the target at angles relative to the $\bar{p}$ beam of 60°, 30°, 15°, 0°, and −15°, respectively. The neutron detectors consisted of liquid NE213 scintillators with a thickness of 10.16 cm and a diameter of 10.16 or 12.7 cm. The detector $N4$ was 25.4 cm thick in order to stop also highly energetic $\pi^{\pm}$ and $K^{\pm}$. The scintillator NE213 has special pulse-shape properties which were exploited to discriminate between weakly ionizing particles like e^- produced by γ rays, $\pi^{\pm}$, $K^{\pm}$, which were not stopped, from strongly ionizing particles like stopped p, d, t, and stopped $K^{\pm}$. Neutrons produce strongly ionizing parti-

cles from n-p scattering and reactions induced in carbon of the organic NE213 scintillator. The pulse-shape signal ΔE was obtained from the difference of the fast and slow components of the dynode signal of the multiplier viewing the NE213 scintillator. The time resolution of the n detectors was 1.0–1.2 ns as measured against the $\overline{S1} \wedge S2$ start. These time resolutions resulted in energy resolutions of 6 MeV for nucleons at 120 MeV. The hardware thresholds for neutrons were set between 1.1 and 2.4 MeV neutron equivalent energy. The efficiency was calculated with the code of Cecil *et al.* [19]. In Fig. 2 we show typical efficiency curves for different thresholds of neutron energy used in this experiment.

In order to separate neutral mesons, γ rays, and neutrons from charged particles, a 3 mm thick scintillator paddle was positioned in front of each neutron detector. In front of $N5$ an additional plastic scintillator of thickness 2.54 and 5.08 cm was used in order to identify $K^{\pm}$ better.

For each detected particle the time of flight $\mathrm{TOF}_{n,p}$ from the target to the paddle (p) and neutron detector (n) was measured in reference to $\overline{S1} \wedge S2$. In addition the deposited energy or energy loss $E_{n,p}$ in the paddle and n detector was measured as well as the pulse-shape signal ΔE_n. These five parameters were written on tape for off-line analysis. The normalization was derived from the integrated number of valid $\bar{p}$'s as given by the total counts of $\overline{S1} \wedge S2$ corrected for the dead time of the data acquisition system.

In Fig. 3 the deposited energy E (light) in one neutron detector is plotted versus the time of flight T_n. The condition for the top panel was a coincident signal in the associated paddle, corresponding to a charged particle, whereas for the lower panel only those events are shown when there was no paddle signal corresponding to neutral particles n or γ rays. In order to obtain a large dynamic range of 1:200, low energies, 1–80 MeV, were derived from the multiplier dynode 14 of an XP2041 multiplier (lower part in each panel) whereas higher energies were obtained from dynode 11 with 10 times smaller gains (upper part in each panel). This plot clearly demonstrates the excellent separation of $\pi^{\pm}$, $K^{\pm}$, p, d, and t as well as γ rays (e^-). In addition to the TOF-E correlation the pulse-shape properties ΔE of the scintillator were exploited.

The energy spectra for neutrons are obtained from the measured time of flight using relativistic relations whereas for charged particle spectra corrections were made for the energy loss in the target, air, paddle, and n-scintillator wall. For $K^{\pm}$ and $\pi^{\pm}$ corrections for the decay in flight were applied as well.

Since stopped antiprotons are captured via atomic orbits, the measured inclusive particle spectra should be isotropic and independent of the initial $\bar{p}$ direction. This was verified by all five neutron detectors. Furthermore, the multiplicity spectra are independent of the distance between the target and the detector, signaling a negligible contribution from secondary reactions in any structural material close to the target, e.g., supports, floor, etc. The background, as obtained from shadow bar measurements, was smaller than 5 – 8 % for neutron energies

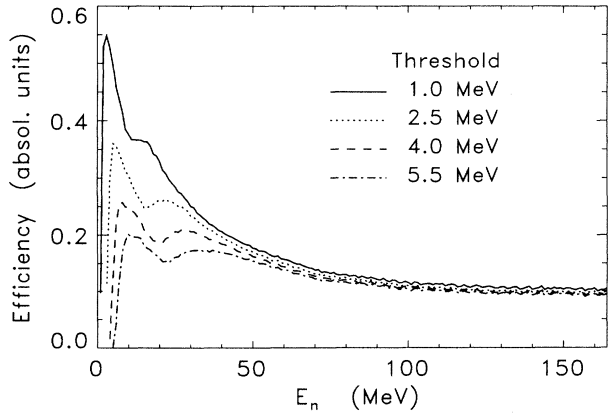

FIG. 2. Comparison of detection efficiencies for several thresholds of neutron energy for a cylindrical detector (diameter × thickness: 12.7 cm × 10.16 cm).

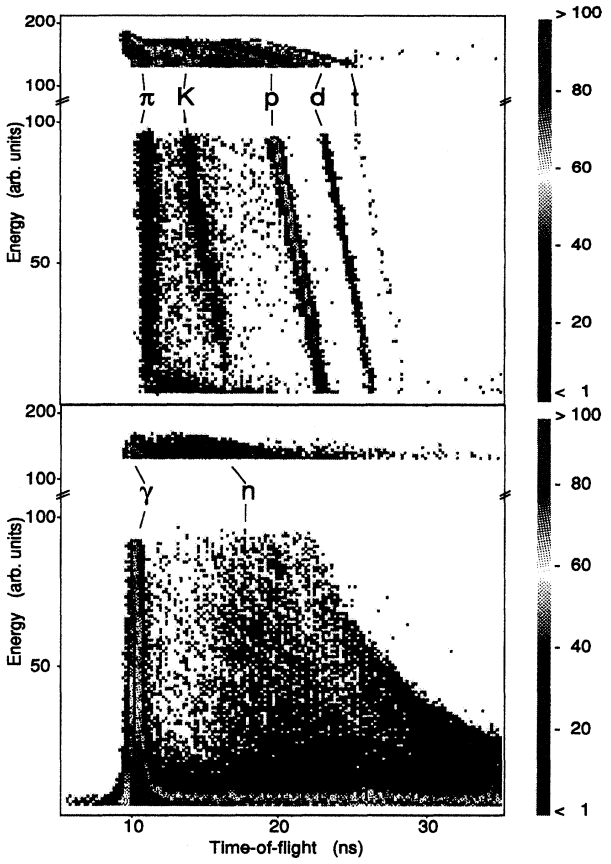

FIG. 3. The energy signal E (recoil energy for neutrons) of the liquid scintillator $N3$ as measured via the light output is plotted versus the time of flight: (a) with a coincidence requirement of the scintillator paddle in front of the liquid scintillator corresponding to charged particles ($\pi^{\pm}$,$K^{\pm}$, p, d, t) and (b) with an anticoincidence corresponding to neutrals (γ and n). The top part in each panel is the offset continuation of the lower part with a reduced energy gain by about a factor of 10.

between 30 and 100 MeV.

The energy spectra for n, p, d, t, $K^{\pm}$, and $\pi^{\pm}$ are shown for uranium in Fig. 4. The neutron spectrum ranges from 2 to 300 MeV. The low energetic evaporation component up to 15 MeV and the high energy preequilibrium between 20 and 250 MeV are clearly visible. Due to energy losses in air, paddle, and the container walls of the scintillator there exists a lower energy cutoff for p, d, t, $K^{\pm}$, and $\pi^{\pm}$, depending on the specific energy loss in the different materials between the target center and the detector. One should, however, note that the energy resolution for $\pi^{\pm}$ is considerably worse than for neutrons: ΔE= 6 and 29 MeV for n and π, respectively, at an energy of 120 MeV. The spectra of charged baryons in Fig. 4, as well as in Fig. 5, show a deviation from the exponential decrease (around 100 MeV for protons) due to a nonlinearity in the anode signal caused by very large light outputs (see Fig. 3), which affected the time of flight deduced from the anode signal. This could not be corrected completely by exploiting the dependence of the γ peak on the energy, i.e., on the light output of the liquid scintillator.

In order to reduce the large amount of data of 4 or 6 particle species from 13 targets and to facilitate comparison with theoretical models, we have parametrized each measured spectrum by a sum of Maxwellian spectral shapes of the form

$$\frac{dM}{dE} = \sum_{i}^{k} \frac{2\langle M_i \rangle}{\pi^{1/2} T_i^{3/2}} \sqrt{E} \exp\left(-\frac{E}{T_i}\right), \quad k = 1,3, \quad (1)$$

with $\langle M_i \rangle$ and T_i as parameters for multiplicity and slope. In the case of charged particles E was replaced by $E - V_C$, where $V_C = 1.44\, Z_{lcp}\,(Z - Z_{lcp} - 1)/(r_0 A^{1/3})$ is the Coulomb barrier of the specific particle (lcp = $\{p, d, t\}$) in each target with mass A and proton number Z; r_0 was taken to be 1.2 fm.

By inspecting the energy spectra of neutrons as shown in Fig. 4, it is obvious that a low (E_n < 15 MeV) and a high (E_n > 40 MeV) energy component is present. These two components can be associated with (a) neutron evaporation from a thermally equilibrated residual nucleus and (b) directly emitted neutrons from the primary π-nucleon interactions. The inverse slope parameter T_i represents the nuclear temperature (a) and the energy distribution of the primary pions in the case of (b).

Closer inspection of the measured n spectra results in a further intermediate component for nuclei heavier than holmium. By allowing in the χ^2 fit for a third source the total χ^2 was reduced by 30%. This third component can be interpreted as preequilibrium emission during the nucleon-nucleon cascade after the primary pion-nucleon interaction. The obtained fit with an evaporative (i = 3), intermediate preequilibrium (i = 2), and a direct neutron source (i = 1) is shown in Fig. 5 for $\bar{p}$ annihilation in ^{197}Au. Without this third source it was not possible to obtain a reasonable description in the energy range between 15 and 35 MeV.

Due to the experimental low energy cutoff for charged particles, we could deduce for charged particles only the parameters for the direct source (1). The fit for protons is also shown in Fig. 5. The parameters obtained for the multiplicities and slope parameters are given in Tables I and II. The multiplicity and the "temperature" parameter of the direct neutron source (1) from this experiment are somewhat smaller than the values for copper and uranium determined in an earlier measurement [6] due to an improved background correction enabled by the increased number of detection angles. The multiplicities for p, d, and t agree reasonably well with previous charged particle measurements by Hofmann *et al.* [9] and (as an extension of the former work) by Sudov *et al.* [10] in a comparable range of emitted energies. The proton spectra for ^{12}C and ^{238}U measured by Minor *et al.* [15] extend the presented spectra to higher kinetic energies.

As indicated in Fig. 3 we have also measured charged pions $\pi^{\pm}$, but due to the insufficient time resolution we do not show energy spectra. For that reason the mean kinetic energies of pions could not be determined directly

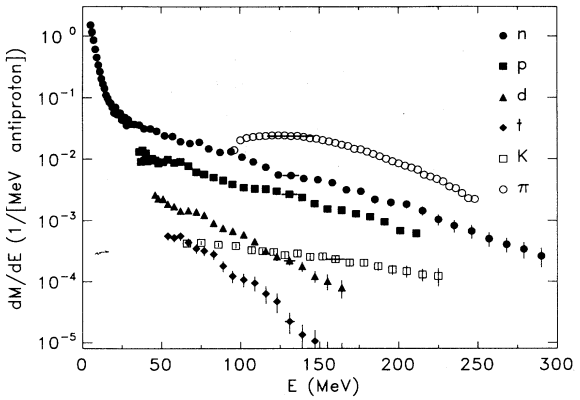

FIG. 4. Energy spectra of all identified particles following antiproton annihilation at rest on uranium. The energy resolution for the particles is shown for an energy of about 120 MeV by horizontal error bars.

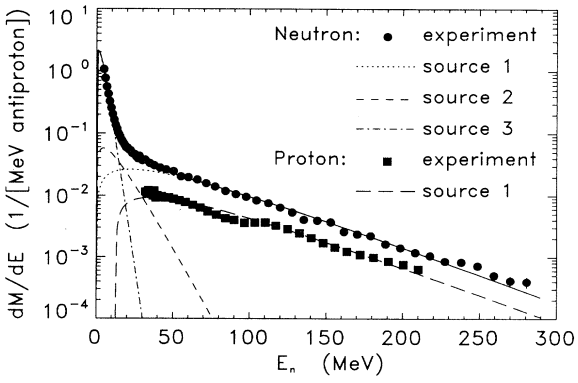

FIG. 5. Differential neutron and proton multiplicities from $\bar{p}$ annihilation on gold. The lines correspond to the various contributions as indicated and described in the text, with parameters from Tables I and II.

TABLE I. Parameters obtained by the multiple-source fits for neutrons: multiplicities M_i and "temperature" T_i [see Eq. (1)].

	Neutron					
	M_1	T_1 (MeV)	M_2	T_2 (MeV)	M_3	T_3 (MeV)
^{12}C	1.37±0.09	46.2±1.6	-	-	0.68±0.16	3.60±0.31
^{27}Al	1.66±0.15	42.1±1.8	-	-	1.42±0.27	3.31±0.34
^{28}Si	1.66±0.11	42.1±1.7	-	-	1.27±0.12	3.24±0.36
^{40}Ca	1.79±0.13	42.1±2.1	-	-	1.49±0.27	3.36±0.36
^{64}Cu	2.20±0.27	40.1±2.1	-	-	3.70±0.31	3.10±0.29
^{92}Mo	2.26±0.17	40.1±1.6	-	-	4.10±0.41	3.24±0.31
^{100}Mo	2.50±0.14	39.0±1.8	-	-	6.49±0.55	3.18±0.33
^{108}Ag	2.29±0.17	40.4±1.8	-	-	5.71±0.66	3.21±0.42
^{165}Ho	2.30±0.23	38.3±1.8	1.09±0.11	8.45±1.04	8.77±0.81	2.60±0.23
^{181}Ta	2.46±0.16	37.4±1.3	1.19±0.13	8.76±0.95	10.3±1.06	2.60±0.28
^{197}Au	2.48±0.15	36.6±1.9	1.13±0.17	7.51±0.89	11.3±0.86	2.60±0.21
^{209}Bi	2.59±0.23	36.3±2.0	1.08±0.19	6.87±1.01	11.9±1.02	2.53±0.31
^{238}U	3.16±0.31	37.7±2.5	1.15±0.21	5.78±0.79	13.8±1.30	2.67±0.20

and we assume for the further analysis $\langle E_\pi^{\rm kin}\rangle = 210$ MeV for the primary pion spectrum [20]. However, from the time-of-flight spectra we could deduce the yield of charged pions directly. The correction for decay in flight was smaller than 3.5%. The $\pi^\pm$ multiplicities are also given in Table III and are compared in Fig. 6 with published values [21,23,24]. The abscissa in the plot represents the probability that a pion produced at a distance $R_{\rm ann} = r_0 A^{1/3} + \frac{1}{2}\delta$ from the nuclear surface will not interact or not be absorbed by the nucleus. The radius parameter r_0 equals 1.2 fm, $\delta = 2.3$ fm corresponds to the surface diffuseness [20], and A is the mass number of the nucleus. The solid angle Ω of the nucleus with respect to the annihilation location is then given on average by

$$\frac{\Omega(A)}{4\pi} = \frac{1}{2}\left[1 - \sqrt{1 - A^{1/3}\Big/\left(A^{1/3} + \frac{\delta}{2r_0}\right)}\right] . \quad (2)$$

TABLE II. Parameters obtained by the multiple-source fits for light charged particles: multiplicities M_1 and "temperature" T_1 from Eq. (1) (the spectra were fitted in the energy range $35 \leq E_p \leq 200$ MeV, $50 \leq E_d \leq 160$ MeV, and $60 \leq E_t \leq 150$ MeV).

	Proton		Deuteron		Triton	
	M_1	T_1 (MeV)	M_1	T_1 (MeV)	M_1	T_1 (MeV)
^{12}C	0.70±0.06	44.5±1.7	0.081±0.008	23.7±1.1	0.020±0.001	19.8±0.9
^{27}Al	0.84±0.07	41.3±2.0	0.097±0.008	25.1±1.2	0.024±0.001	20.3±0.9
^{28}Si	0.86±0.05	43.2±1.7	0.118±0.010	24.4±1.0	0.029±0.004	19.2±0.7
^{40}Ca	0.96±0.07	41.5±1.8	0.127±0.009	24.1±1.1	0.031±0.003	19.0±0.7
^{64}Cu	0.99±0.08	39.1±2.1	0.152±0.013	23.2±0.8	0.042±0.002	18.1±0.8
^{92}Mo	1.05±0.06	38.3±1.7	0.156±0.017	23.2±0.9	0.036±0.002	18.9±0.8
^{100}Mo	0.98±0.07	38.7±1.6	0.155±0.015	22.8±0.8	0.044±0.002	18.2±0.8
^{108}Ag	0.94±0.08	39.5±1.9	0.144±0.011	23.9±1.1	0.036±0.004	19.2±0.8
^{165}Ho	0.89±0.08	38.4±1.6	0.137±0.012	23.0±0.9	0.037±0.003	18.6±0.8
^{181}Ta	0.91±0.09	37.4±1.5	0.126±0.017	23.7±0.9	0.028±0.003	17.9±0.8
^{197}Au	0.93±0.09	36.9±1.8	0.120±0.010	22.5±0.8	0.030±0.004	17.7±0.7
^{209}Bi	0.92±0.08	38.2±2.2	0.119±0.014	22.6±0.9	0.029±0.002	17.7±0.7
^{238}U	1.04±0.12	37.7±2.4	0.140±0.011	22.6±1.0	0.044±0.004	17.5±1.1

TABLE III. Multiplicity for charged pions, deduced from the time-of-flight spectra.

	$M_{\pi\pm}$
^{12}C	2.77 ± 0.08
^{27}Al	2.68 ± 0.07
^{28}Si	2.64 ± 0.08
^{40}Ca	2.59 ± 0.06
^{64}Cu	2.53 ± 0.07
^{92}Mo	2.49 ± 0.06
^{100}Mo	2.51 ± 0.06
^{108}Ag	2.51 ± 0.08
^{165}Ho	2.46 ± 0.08
^{181}Ta	2.48 ± 0.08
^{197}Au	2.47 ± 0.08
^{209}Bi	2.46 ± 0.07
^{238}U	2.41 ± 0.06

The number of pions $\langle M_{\pi\pm}\rangle$ which are not absorbed by the nucleus is given by

$$\langle M_{\pi\pm}\rangle = \langle M_{\pi^\pm}^{\rm prim}(1-\Omega/4\pi)\rangle, \quad (3)$$

with $\langle M_{\pi^\pm}^{\rm prim}\rangle$=3.1 [20] being the primary charged pion multiplicity produced in the $\bar{p}$-nucleon annihilation process. The long dashed line in Fig. 6 corresponds to this simple relation whereas the dash-dotted curve indicates $\langle M_{\pi^\pm}^{\rm prim}\rangle$.

In addition to charged pions we have measured charged kaons in a restricted energy interval of 60–200 MeV. The measured yield was corrected for decay in flight. The kaon spectra were fitted with a relativistic Maxwell-Boltzmann distribution [25]

$$\frac{dM}{dE} = B\,p\,\exp\left(-\frac{E}{T_{K^\pm}}\right), \quad (4)$$

with p the kaon momentum and B a normalization constant which yields the kaon multiplicity $M_{K^\pm}$. The result is shown in Fig. 7; in addition we show the measured multiplicity in the energy interval 60–200 MeV. The deduced "temperature" parameters $T_{K^\pm}$ give the mean kinetic energies for further analysis.

In Figs. 8 and 9 the multiplicities of evaporated neutrons and directly emitted neutrons and protons are shown. In Fig. 10 the ratios of the deuteron and triton yield relative to the proton yield are shown as a function of A. We observe in Fig. 8 an almost linear increase of the evaporated neutron multiplicity with mass number which indicates an increase of the deposited excitation energy with A. The increase of neutron multiplicity with A is enhanced since at high A most of the thermal energy is carried away by neutron evaporation, whereas at low A a considerable fraction of the thermal energy goes also into charged particle evaporation due to a smaller Coulomb barrier. This will be treated in more detail in Sec. III. For the directly emitted highly energetic p, d, t, we observe that the multiplicity is almost independent of A and amounts, respectively, to 1, 0.15, 0.03, whereas for the directly emitted neutrons we observe a strong increase from about 1.5 neutrons at $A = 12$ to 3 neutrons at $A = 238$. This increase is considerably stronger than one would expect from the neutron-to-proton ratio in the target nuclei which increases, respectively, from 1.0 to 1.59. This will be discussed in more detail in Sec. IV.

One might argue that an unexpected ratio in the measured neutron-to-proton yield might be due to imperfectly known neutron detection efficiencies. As mentioned above we have used the code of Cecil *et al.* [19] and we show an efficiency curve in Fig. 2. In order to check the detection efficiencies used we have performed two tests:

(i) We have excluded possible effects of the light response function using different neutron thresholds (1.1–

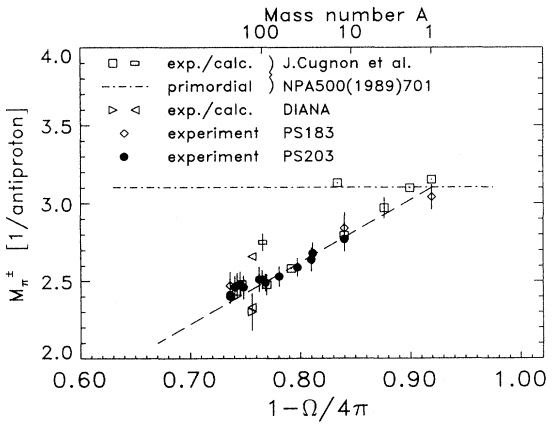

FIG. 6. The average number of charged pions of the experiments PS203 (this work), PS183 [23], and the DIANA Collaboration [24] together with a compilation of Cugnon and Vandermeulen [21] as a function of solid angle $(1-\frac{\Omega}{4\pi})$ of noninteraction [see text and Eq. (2)].

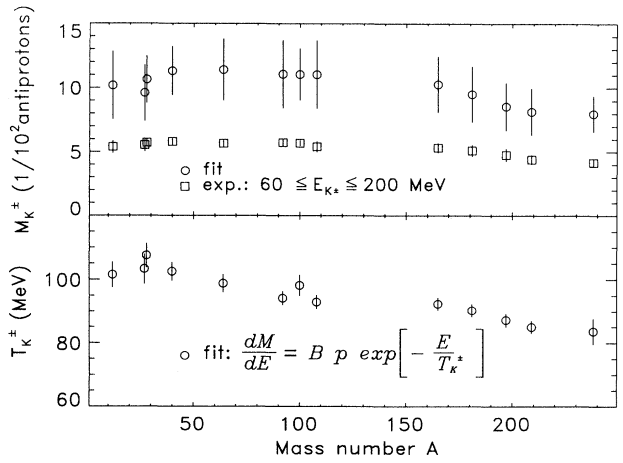

FIG. 7. Multiplicities of charged kaons (upper panel), deduced from integration of the experimental spectrum over the given and the whole energy range, respectively (based on a fit to the spectra), and the "temperature" parameters of these spectra (lower panel) as function of the target mass.

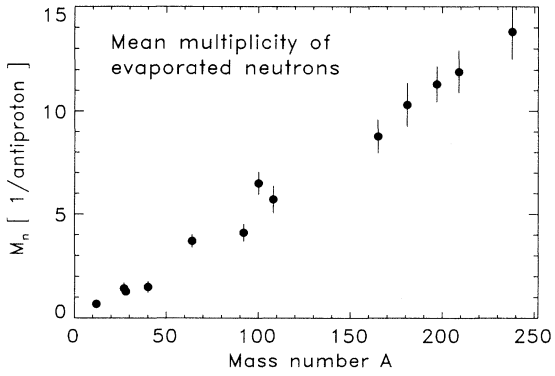

FIG. 8. Multiplicity M_3 of evaporated neutrons as function of target mass.

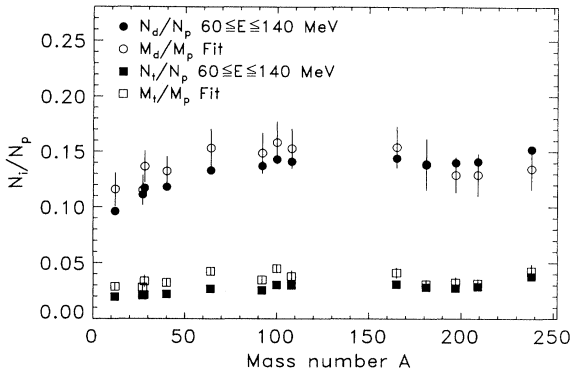

FIG. 10. Yields of deuterons and tritons relative to protons as a function of target mass. The ratios were deduced from the experimental spectra in the given energy range and from the fitted multiplicities given in Table II, respectively.

2.4 MeV).

(ii) We have calibrated the efficiency of the neutron counters by detecting neutrons only via n-p scattering in the scintillator by exploiting the pulse-shape properties which enabled us to identify reactions on carbon in the organic scintillator. For details see Polster *et al.* [26]. From these cross-checks we conclude that the error for the used n-detection efficiencies is smaller than ±8%.

III. ENERGY DISSIPATION

The process of energy dissipation is decisive for the formation of hot nuclei following $\bar{p}$ annihilation at rest. Energy balance for the antiproton annihilation on a proton of the nucleus ${}^{A}_{Z}X$ leads to

$$m_{\bar{p}} + M(Z,A) - M(Z-1,A-1)$$

$$= \langle E_\pi \rangle + \langle E_K \rangle + \langle E_n \rangle + \langle E_{lcp} \rangle + \langle E_\gamma \rangle, \quad (5)$$

with $m_{\bar{p}}$ the antiproton mass, $M(Z,A) - M(Z-1,A-1)$ as atomic mass difference, and $\langle E_\pi \rangle$ and $\langle E_K \rangle$ the total energies (inclusive rest masses) of emitted pions (or pionic resonances) and strange particles, respectively. The total energies including binding energies for neutrons and light charged particles are denoted by $\langle E_n \rangle$ and $\langle E_{lcp} \rangle$. $\langle E_\gamma \rangle$ is the energy emitted by γ rays.

This global energy balance can be investigated following the subsequent stages of the antiproton-nucleus interaction employing observables determined in this experiment. The presented measurements allow a more direct approach as done for the uranium case in [22].

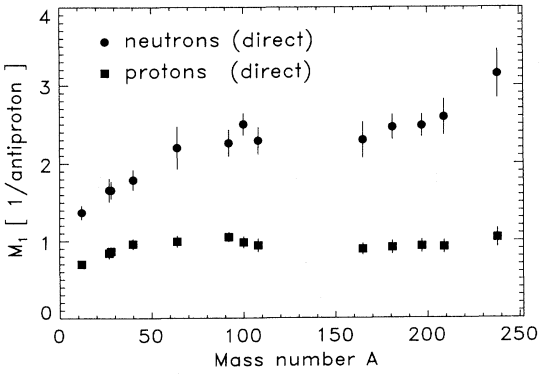

FIG. 9. Multiplicity M_1 of directly emitted nucleons in dependence on target mass.

A. Energy transfer

The spectra of emitted mesons, especially pions, shed light on the first stage of energy dissipation from the pionic system (formed in annihilation) to the baryonic system of $A-1$ nucleons. The multiplicity difference between primordial and in the experimentally observed pions is a direct measure of that part of the annihilation energy transferred to the target nucleus.

The experimental yields $\langle M_i \rangle$ and mean kinetic energies $\langle E_i^{\rm kin} \rangle$ of charged pions and kaons (to which neutral mesons are added) allow the determination of the mean fraction $E_{\rm trans}$ of the initially available energy transferred from the multipion system to the nucleus:

$$E_{\rm trans} = 2m_N c^2 - \sum_{i=\pi,K} \langle M_i \rangle [\langle E_i^{\rm kin} \rangle + m_i c^2] \quad . \quad (6)$$

The results of our analysis are shown in Fig. 11 together with values of the PS183 Collaboration (strange particles are neglected in the analysis of [23,27] and in some theoretical predictions [28–30]. The observed saturation of transferred energy with increasing target mass supports the simple geometrical arguments for the interaction of the annihilation products with the nucleus (see Sec. II).

The energy, which is transferred from the primordial mesonic system to the nucleus, will, however, not be ab-

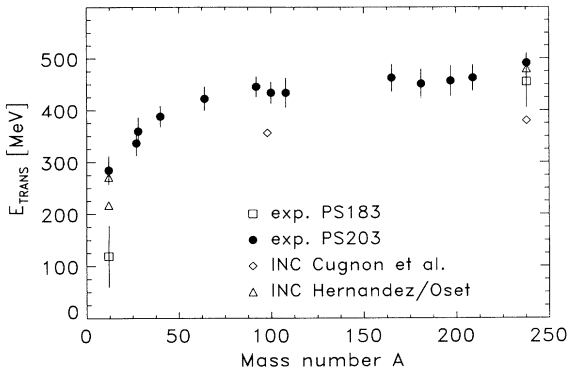

FIG. 11. The target mass dependence of the mean energy $E_{\rm trans}$ from experiments (PS203 this work and PS183 [23] and INC calculations by Cugnon and co-workers [28,29] and Hernandez and Oset [30]).

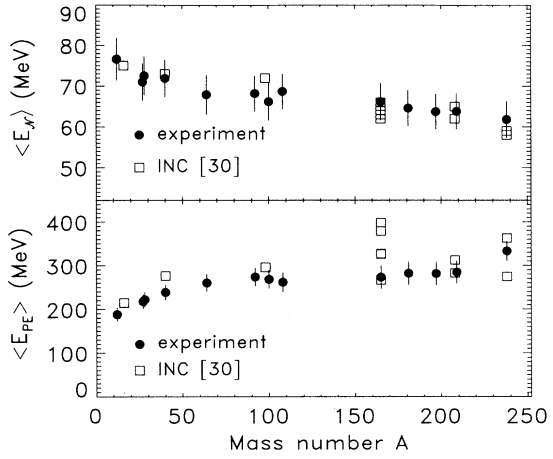

FIG. 12. Mean kinetic energy per nucleon $\langle E_N \rangle$ emitted during the cascade (upper panel) and mean preequilibrium energy $E_{\rm PE}$ (lower panel) in dependence on target mass. The INC calculations were performed in [29] for some nuclei with different annihilation radii or annihilation states.

sorbed completely by the interacting nucleus as internal excitation energy. For the determination of thermal excitation after the fast intranuclear cascade this method of missing annihilation energy lacks the (important) information of the energy carried off by fast baryons before thermal equilibrium is achieved. The determination of this energy requires the analysis of all particles (in particular nucleons) emitted during the fast stage of the reaction.

B. Cascade and preequilibrium emission

The present experiment provides an approach to this ideal case via the nucleon and light complex particle spectra deduced. These are characterized by the mean multiplicity $\langle M_i \rangle$ and kinetic energy $\langle E_i^{\rm kin} \rangle$ determined from Eq. (1) by $\langle E_i^{\rm kin} \rangle = \frac{3}{2} T_i$. These observables yield the preequilibrium energy $E_{\rm PE}$ emitted prior to the attainment of thermal equilibrium,

$$E_{\rm PE} = \sum_{i=n,p,d,t} \langle M_i \rangle [\langle E_i^{\rm kin} \rangle + B_i], \tag{7}$$

where B_i is the binding energy of particle i. The consideration of ^{3}He and α emission measured in [8] in the energy balance increases $E_{\rm PE}$ by about 0.6% only. This value is much smaller than the statistical error of $E_{\rm PE}$.

Not only the energy $E_{\rm PE}$, but also the mean kinetic energy of nucleons emitted during the intranuclear cascade,

$$\langle E_{\mathcal{N}} \rangle = \frac{\sum_{i=n,p} \langle M_i \rangle [\langle E_i^{\rm kin} \rangle + B_i]}{\sum_{i=n,p} \langle M_i \rangle}, \tag{8}$$

is in reasonable agreement with INC predictions as shown in Fig. 12. The mean energy of nucleons decreases with increasing target mass due to the larger number of participating target nucleons.

The large amount of transferred energy (more than 50%) carried away before an equilibrated nucleus is formed emphasizes the importance of the cascade and preequilibrium processes.

C. Mean excitation energy of the compound nucleus

The excitation energy E^* retained by the nucleus following the fast pion interaction and preequilibrium processes ($\tau \preceq 10^{-22}$ s) can be obtained as the difference of the transferred energy $E_{\rm trans}$ and the energy $E_{\rm PE}$:

$$E^* = E_{\rm trans} - E_{\rm PE} \quad . \tag{9}$$

A second, independent, and more precise method to deduce the thermal energy of the excited nucleus is based on the measured energy spectra of evaporated neutrons. The yield and the shape of these spectra are compared to calculations which were performed with a statistical model [31] in order to take into account the unmeasured energy carried away by evaporated light charged particles.

The excitation energies deduced by these different methods are shown by open circles and solid squares and are compared to INC calculations by Cugnon *et al.* [32] and Ijinov *et al.* [20] in Fig. 13. Both methods agree quite well especially for medium and heavy targets. The nuclear excitation by means of $\bar{p}$ annihilation at rest seems to saturate with increasing target mass at mean values between 150 and 200 MeV.

Each of the three discussed observables $\langle E_{\rm trans} \rangle$, $\langle E_{\rm PE} \rangle$, and $\langle E^* \rangle$ shown in Fig. 14 represents a different time regime of the $\bar{p}$-nucleus interaction. These "static" observables correspond very nicely to the dynamical picture of energy dissipation drawn by INC simulations (Fig. 15). The mean excitation energy of a lead nucleus increases during the first πN collisions and reaches after a time of about 8 fm/c a maximum around 450 MeV

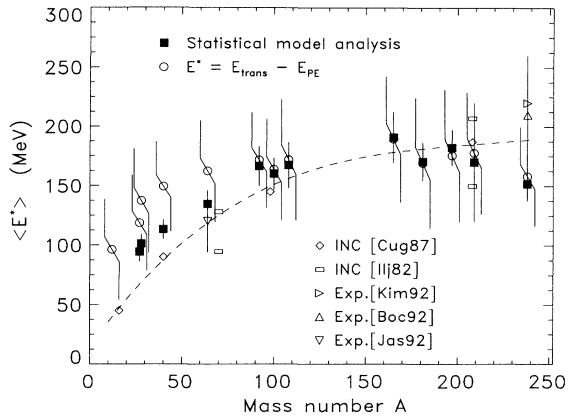

FIG. 13. Target mass dependence of the experimentally determined excitation energy deposited in the decaying nucleus E^* by two methods (see text) from this experiment compared with INC calculations [20,32]. The dashed line is drawn through the calculated INC values. The other experimental data [7,11,33] are deduced from the mass loss of the reaction products, which represents only a relative measure of the excitation energy, because a mean energy per emitted mass unit is needed (in this work, however, we could distinguish between directly emitted and evaporated particles).

corresponding to the experimentally deduced observable $\langle E_{\rm trans}\rangle$ in the upper panel of Fig. 14. The nucleus then cools down during the proceeding cascade and via preequilibrium processes emitting on average more than half of the transferred energy. The energy emitted during this stage corresponds to a measured preequilibrium energy

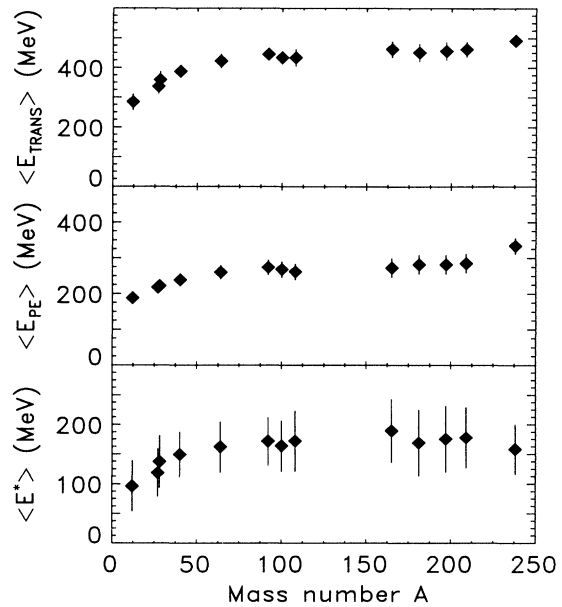

FIG. 14. Target mass dependence of the mean energy $E_{\rm trans}$ transferred from the multipion system to the nuclear system (top panel), of the energy $E_{\rm PE}$ emitted prior to thermal equilibrium (middle panel), and of the mean excitation energy E^* gained by the compound nucleus (lower panel), respectively.

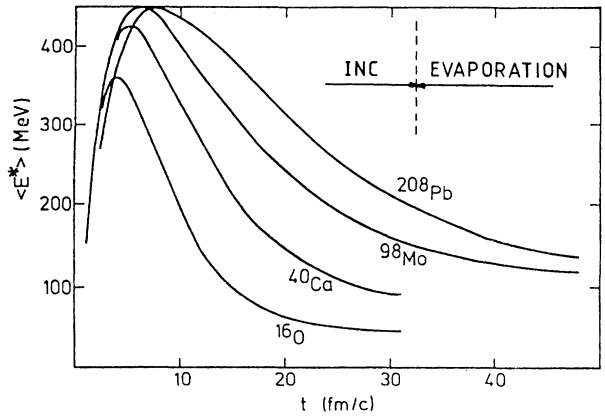

FIG. 15. Time dependence of the mean energy dissipation after $\bar{p}$ annihilation on different target nuclei. The figure is adopted from Cugnon *et al.* [32].

$\langle E_{\rm PE}\rangle$ of about 270 MeV for ^{209}Bi in the middle panel of Fig. 14. Finally, after about 30 fm/c (about 10^{-22} s) the nuclear system is equilibrated and evaporates particles (mainly neutrons) and finally undergoes either fission or survives as a heavy residue.

In the case of antiproton annihilation at rest on nuclei we can state that the gross features of the formation of hot nuclei are understood by the dynamics of an intranuclear cascade combined with a simple geometrical picture for the interaction between the multipion system and the target nucleus. The study of selected, more sensitive observables characteristic of a specific stage of the antiproton-nucleus interaction should extend the physical understanding of this complex process.

IV. RATIO OF ENERGETIC NEUTRONS TO PROTONS

The emission of fast nucleons is a suitable observable for a more detailed investigation of the intranuclear cascade initiated by the annihilation products. The highly energetic neutrons and protons are associated with the early stage of the interaction between the pionic and baryonic systems. Especially the ratio of emitted neutrons to protons measured simultaneously in one experiment provides a qualitative new observable which allows the study of nonequilibrium effects on a "linear scale" in contrast to the exponentially decreasing particle spectra.

The ratio of energetic neutrons to protons can be determined from the mean multiplicities $\langle M_1\rangle$ (see Tables I and II or Fig. 9). The ratio

$$R = \frac{\langle M_{1,n}\rangle}{\langle M_{1,p}\rangle} \tag{10}$$

and the "normalized" ratio $R/(N/Z)$ taking into account the different numbers of neutrons (N) and protons (Z) in the 13 targets investigated are shown in Fig. 16. The multiplicity ratio R increases with N/Z of the target;

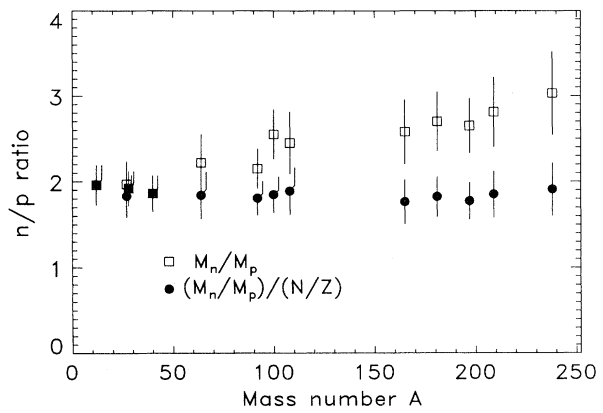

FIG. 16. Neutron-to-proton ratio R of the highly energetic component [see Eq. (10)] in dependence on mass of the target nucleus and R normalized to the respective N/Z ratio.

however, it is about twice the N/Z ratio and nearly independent from the target mass. The neutron-to-proton ratio for the isotopes ^{92}Mo and ^{100}Mo for instance is nearly identical after normalization for N/Z.

The total neutron multiplicities $\langle M_{1,n}\rangle$ and $\langle M_{1,p}\rangle$ given in Tables I and II were obtained by Eq. (1) and thus contain for protons a suppression due to the Coulomb barrier V_C and an extrapolation to low energies where no data were measured. If one wants to exclude the extrapolation of the direct source [$i = 1$ in Eq. (1) and in Fig. 5] to smaller nucleon energies, one should integrate numerically the energy differential nucleon multiplicities dM_N/dE for energies larger than an appropriate energy. For $E \geq 50$ MeV we obtain for uranium a neutron-to-proton ratio of 2.16 instead of $R = 3.04$ from Eq. (10).

These experimental observables are derived from the simple expectations that the n/p ratio should be equal to the N/Z ratio in the target nucleus. By combining spectra for neutrons [14] and protons [15] from different experiments one gets an even larger value for R from $\bar{p}$ annihilation at rest of 5.8 ± 1.2 .

This global deviation of the ratio of directly emitted neutrons to protons from the N/Z ratio in the target requires a more detailed study. Several effects can influence the particle emission mechanisms. Among these are (i) isospin dependence of $\bar{p}$-annihilation cross sections on a nucleon, (ii) πN interactions (scattering and absorption) in the nuclear medium, (iii) preequilibrium processes, (iv) nuclear-structure-dependent nucleon densities $\rho_n/\rho_p(r)$, and (v) Coulomb effects.

These effects are only partly involved in the established INC models [20,21,34]. Before analyzing the ratio of fast neutrons to protons in the complete framework of an intranuclear cascade model, the influence of the pion-nucleus interaction (ii) under consideration of (i) and (iv) will be discussed in a transparent way.

A. Model of "first interaction"

This simple approach [35] is based on the following assumptions:

(a) The high energy part of the nucleon spectra consists mainly of directly emitted particles from first πN interactions.

(b) The πN interaction being quasifree, the relative strength of cross sections is determined only through the isospin coupling of initial to final state, described by Clebsch-Gordan coefficients.

(c) In the isobar picture for pion scattering,

$$\pi + N \longrightarrow \Delta, \quad \Delta \longrightarrow N', \tag{11}$$

and pion absorption,

$$\pi + N_1 \longrightarrow \Delta, \quad \Delta + N_2 \longrightarrow N_1' + N_2', \tag{12}$$

the $\Delta(3,3)$ resonance dominates.

An excess of neutrons at the nuclear periphery as a consequence of an observed neutron halo [36,37] should influence the initial charge distribution as well as the interaction probability of annihilation pions with neutrons or protons. A density distribution larger than N/Z for $r > R_{1/2}$ with $R_{1/2} = r_0 A^{1/3}$ as the mean square radius increases the ratio of the statistical probability for annihilation on a neutron $[\omega(\bar{p}n)]$ and on a proton $[\omega(\bar{p}p)]$ of the target nucleus with mass A:

$$J = \left.\frac{\omega(\bar{p}n)}{\omega(\bar{p}p)}\right|_A . \tag{13}$$

This leads to an excess of negative charge in the primordial multipion system which would increase (from arguments of isospin coupling) the probability for directly knocked-out neutrons relative to that of protons.

The n/p ratio may also be enhanced by the larger probability for the "first interaction" of the produced pions with a neutron on the periphery of the nucleus, simplified by an effective nucleon density at the point of πN interaction:

$$K = \frac{N_{\text{eff}}}{Z_{\text{eff}}} \stackrel{!}{=} \left.\frac{\rho_n(r)}{\rho_p(r)}\right|_{r>R_{1/2}} . \tag{14}$$

Taking into account explicit isospin coupling [35], the n/p ratio shows a sharper increase for π scattering (which is dominating in the first interaction) than for π absorption on two nucleons. Using assumptions (a)–(c) we get the ratio of fast neutrons to protons shown in Fig. 17 as a function of J and K.

This ratio in our simple approach is comparable to the experimental results ($R \approx 2, \ldots, 3$) only for very large K (about 5) and J values. The latter especially would increase the π^-/π^+ ratio in contradiction to the experimental findings [23]. The K values are also unrealistically larger than N/Z because these correspond to very peripheral annihilations. These events, however, do not yield a substantial amount of directly knocked-out nucleons.

In summary, the experimental neutron-to-proton ratios cannot be explained by this simple "first interaction" approach.

A more detailed study, recently done by Van den Bossche and Vandermeulen [17], deals with the simple cascade of scattered pions and includes in a second step also pion

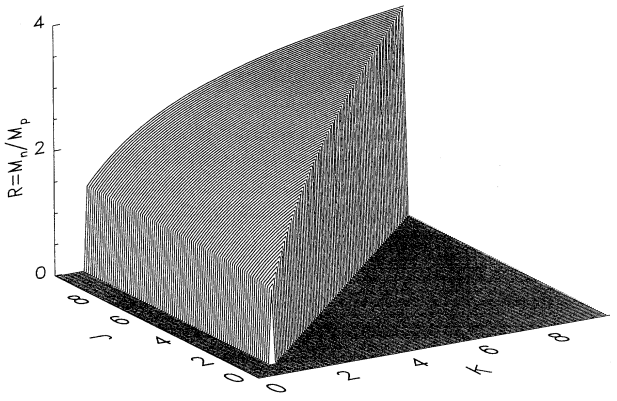

FIG. 17. Dependence of the neutron-to-proton ratio R from locally varying nucleon densities (on the x axis the "effective" N/Z ratio K, on the y axis annihilation parameter J; for details see text).

absorption as in Eq. (12). The results of this approach are significantly lower for lighter targets than the experimental data. In Fig. 18 the experimental ratio

$$R^* = \frac{M_{1,n} + M_{1,d} + 2 \cdot M_{1,t}}{M_{1,p} + M_{1,d} + M_{1,t}} \tag{15}$$

is shown, taking into account the emitted nucleons bound in light complex particles which can decrease the n/p ratio slightly [38]. The calculation [17] does not distinguish between bound or unbound emitted nucleons. They finally concluded that the ratio of highly energetic neutrons to protons cannot be understood in the simple scheme of πN interactions only.

For that reason a detailed investigation [18] was performed on the basis of a complete INC framework including the momentum distribution of pions, the Pauli principle, and the kinematics of the process.

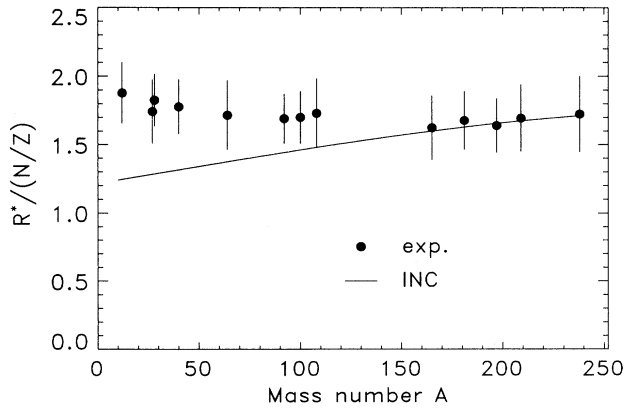

FIG. 18. Experimental ratio R^* of fast neutrons to protons [see Eq. (15)] in comparison to INC calculations [17].

B. Intranuclear cascade model

The INC model was used extensively for the interpretation of several features of antiproton annihilation on nuclei. However, the only published calculation of the neutron spectrum for uranium [29] shows a very good agreement with the experimental spectrum presented here. The stated underestimate of the experimental n/p ratio by the theory was discussed up to now for mean particle multiplicities. The measured nucleon spectra allow, in addition, the analysis of the corresponding ratio of directly emitted neutrons to protons as a function of (nucleon) energy:

$$R'(E) = \frac{dM_{1,n}/dE}{dM_{1,p}/dE}. \tag{16}$$

As a starting point for the theoretical analysis an INC model in its standard version [20] was used, i.e., without consideration of the "trawling" (see Fig. 19). The nonlinear trawling effect takes into account the depletion of the nuclear density during the development of the cascade

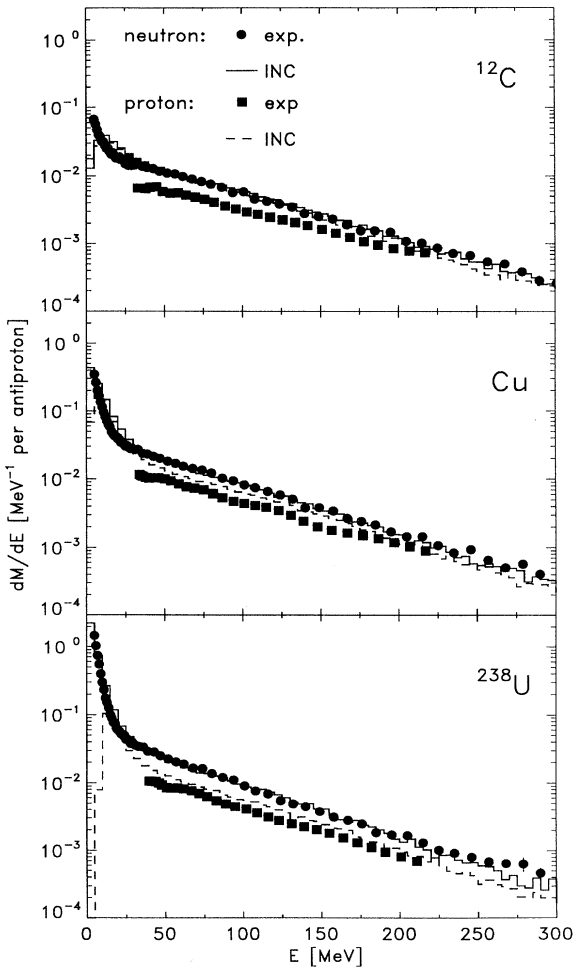

FIG. 19. Experimental nucleon spectra compared to results of the INC model in its standard version.

[39]. The enhancement for proton spectra noted before in [10] could be diminished by taking into account the "trawling" effect. This leads, however, to inconsistencies for d and t spectra, maybe due to uncertainties of the coalescence approach used. In the present work the influence of isospin coupling for pion absorption $\pi+\mathcal{NN} \rightarrow \mathcal{NN}$ on the energy-dependent n/p ratio $R'(E)$ was investigated.

The resulting n/p ratios from complete INC calculations [18] with isospin effects are shown in Fig. 20 for carbon, copper, and uranium in comparison with this experiment. The calculated ratios are around the N/Z ratios of target nuclei, nearly independent of the emitted nucleon energy.

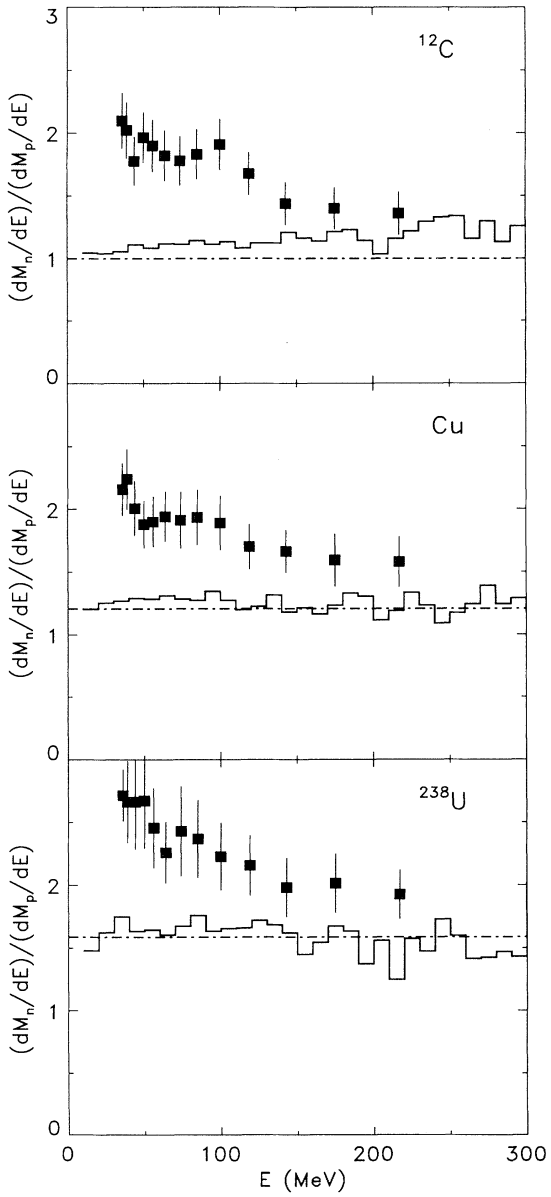

FIG. 20. Comparison of the measured neutron-to-proton ratio for $\bar{p}$ annihilation at rest on ^{12}C, ^{nat}Cu, and ^{238}U with the corresponding INC calculations (histograms) [18]. The error bars give the statistical error and the error due to the imperfectly known efficiency of neutron detection. The limited time resolution (i.e., the uncertainty of the nucleon energy) yields to an additional error (at 120 MeV up to 11%).

Besides isospin effects, two-nucleon annihilations as well as a possible neutron halo can influence the emission of fast nucleons. From the analysis of highly energetic proton spectra [40] a fraction of 5% $\bar{p}\mathcal{NN}$ annihilations was determined which indicates no significant effect on the n/p ratio from the INC model [18].

The inclusion of a neutron halo depends strongly on its parametrization. In a work of Sibirtsev [41] the calculated (energy integrated) n/p ratios are comparable with the experimental ones under an extreme assumption. In the nucleus the local nucleon densities are identically $[\rho_n(r) \equiv \rho_p(r)]$. The whole neutron excess $N-Z$ should be located in a "neutron belt" of thickness t (about 1.2 fm) on the nuclear periphery. Such a formal "neutron belt" corresponds, however, conceptionally closer to a "neutron skin" than to a halo in contrast to the experimental results [37].

C. Further concepts

The INC model without consideration of quite unrealistic effects of nuclear structure cannot reproduce the very sensitive ratio of fast neutrons to protons. The reason seems to be the nonconsistent description of light charged particles because the absolute intensity for protons from the calculation is too large. The effects of two-nucleon annihilation and isospin discussed here as well as the influence of meson resonances (ω and η) mentioned in [17], as also taken into account in [18], cannot resolve the discrepancies between the experimental and calculated ratios.

The deviation of n/p ratios from $\bar{p}$ annihilation at rest from π- or p-induced reactions points to a possible anisotropy of the primary "pion cloud," formed in annihilation, in contrast to a $\pi^{\pm}$ beam. A small anisotropy may be caused by the nuclear Coulomb field. The π^- mesons of the primary pion distribution will be focused to the target nucleus whereas the spatial π^+ distribution will be deformed to larger radii. This would give a larger interaction probability with target nucleons for π^- than for π^+, leading to a sharp increase of the ratio of fast neutrons to protons as discussed above.

A further physical effect is conceptually outside the scope of the intranuclear cascade model. This model describes only the subsequent two-body collisions and neglects the action of the nuclear mean field, normally decomposed in a Skyrme type, a Coulomb, and a so-called symmetry potential. The combination of these two pictures leads to the Boltzmann-Uehling-Uhlenbeck (BUU) concept [43] based on the BUU equation.

In the analysis of highly energetic neutron and proton data from the heavy-ion-induced reaction ^{12}C + ^{165}Ho at 31.6 MeV/nucleon [42] a BUU code [44] with isospin-dependent $\mathcal{NN}$ cross sections and a fully isospin-dependent mean potential was used. The calculations [45] show that the enhancement of fast neutron emission

is mainly caused by the isospin dependence of the mean field, especially the symmetry potential. This is contrary to the suggestion that the neutron enhancement might be due to the isospin-dependent $\mathcal{NN}$ cross section [46].

A similiar influence in the case of antiproton annihilation at rest is possible, because the deviation of the experimental n/p ratio from the calculated values is largest at medium energies from 60 to 150 MeV (see Fig. 20). The importance of the dominating $\mathcal{NN}$ collisions at high energies will be blocked at decreasing energies by the Pauli principle. In the same energy region the influence of the mean potential increases. The symmetry potential U_S is normally used in the form [47–49]

$$U_S = C\frac{\rho_n - \rho_p}{\rho_0}\tau \ , \tag{17}$$

where τ is the isospin operator with eigenvalues of ± 1 for neutrons and protons, respectively, ρ, ρ_p, and ρ_n are the nucleon, proton, and neutron densities, and $C > 20$ MeV [45,48–50] is the strength of this potential. The effect of the symmetry potential U_S can be enhanced by an increasing value of $\rho_n - \rho_p$ expected at the periphery of the nucleus.

Therefore, a completely isospin-dependent description of the antiproton-nucleus interaction by transport-theoretical models on the basis of the BUU equation or quantum molecular dynamics (QMD) is needed for further investigation of the problem of enhanced neutron emission.

V. CONCLUSIONS

The formation process of hot nuclear matter following antiproton annihilation at rest was investigated for a wide range of targets from $A = 12$ to 238. By analyzing the measured inclusive multiplicities and spectra of charged mesons, neutrons, protons, deuterons, and tritons, the nonequilibrium stage of the antiproton-nucleus interaction was studied extensively.

The ratio of emitted neutrons to protons determined from the mean multiplicities of the highly energetic part of the spectra was found to be about twice the N/Z ratio for all 13 target nuclei. This deviation from the naive expectation cannot be understood completely in the established framework of the INC model. Especially for nuclei lighter than $A \approx 100$ a mass dependence of the n/p ratio was found which differs from theoretical calculations [17].

The simultanously measured nucleon spectra allow for the first time the observation of the neutron-to-proton ratio as a function of (nucleon) energy for the different targets. In a detailed analysis it was shown that neither the explicit isospin consideration, a realistically parametrized neutron halo, nor two-nucleon annihilations have a significant influence on the neutron-to-proton ratio from an intranuclear cascade based on πN and $\mathcal{NN}$ collisions.

A transport-theoretical description, i.e., BUU or QMD model, including a fully isospin-dependent mean potential could perhaps explain the enhanced neutron emission following antiproton annihilation. Such a description was successful in the case of a heavy-ion reaction at medium energies [45]. The effect of the dominating symmetry potential can be enhanced by a larger $\rho_n - \rho_p$ at the nuclear periphery where the annihilation at rest preferentially takes place. In addition the nuclear Coulomb potential can affect the fast n/p ratio. A transport approach for the inverse physical process, the antiproton production in p-nucleus and nucleus-nucleus collisions, shows reasonable agreement with the experimental results [51].

Besides the nucleon spectra the ratios of light charged particles (d/p, t/d but also d/n) allow the investigation of the entropy production in those reactions. An interconnection between such ratios and the number of participating degrees of freedom was first suggested by Siemens and Kapusta [52] for heavy-ion reactions. In contrast to these reactions the experimental ratios from $\overline{p}$ annihilation at rest are not contaminated by breakup particles.

The experimental findings on energy dissipation, extracted by the deduced mean transferred, preequilibrium, and excitation energies, agree very well with detailed INC predictions [21]. We have shown that for stopped antiprotons only about 10% of the annihilation energy on average attains thermal equilibrium inside the nucleus. The distribution of the excitation energy, however, is very broad, extending from a nearly unexcited nucleus in very distant annihilations up to more than 800 MeV. In the region of the excitation energies gained after $\overline{p}$ annihilation at rest, evaporation and fission are the dominant decay channels, as illustrated by Gross *et al.* [53] for uranium. In order to induce multifragmentation for this nucleus excitation energies above 600 MeV are required; i.e., at mean excitation energies obtained for stopped $\overline{p}$, only a small fraction of events will undergo multifragmentation. The decay of such hot nuclei at very low momenta as a result of antiproton annihilation is the subject of a qualitatively new experiment at LEAR (PS208) [54]. We hope that this experiment will solve some of the open questions related to the decay of very hot nuclei at low spins and low compression.

ACKNOWLEDGMENTS

The excellent antiproton beam due to the outstanding work of the LEAR team is appreciated. We wish to thank H. Daniel for support. Two of us (H.M. and H.S.P.) are grateful for support by a NATO grant (Scientific affairs).

[1] D. Guerreau, in *Nuclear Matter and Heavy Ion Collisions*, edited by M. Soyeur, H. Flocard, B. Tamain, and M. Porneuf (Plenum, New York, 1989), p. 187.

[2] D.H.E. Gross, Rep. Prog. Phys. **53**, 605 (1990).

[3] L.G. Moretto and G.J. Wozniak, Annu. Rev. Nucl. Part. Sci. **43**, 379 (1993).

[4] E. Suraud, M. Pi, P. Schuck, B. Remaud, F. Sebille, C. Gregoire, and F. Saint-Laurent, Phys. Lett. B **229**, 359

(1989).
[5] T. von Egidy, Nature (London) **328**, 773 (1987).
[6] D. Polster and D. Hilscher, Yad. Fiz. **57**, 1698 (1994) [J. At. Nucl. **57**, 1628 (1994)].
[7] J. Jastrzebski *et al.*, Phys. Rev. C **47**, 216 (1993).
[8] W. Markiel *et al.*, Nucl. Phys. **A485**, 445 (1988).
[9] P. Hofmann *et al.*, Nucl. Phys. **A512**, 669 (1990).
[10] A.S. Sudov *et al.*, Nucl. Phys. **A554**, 223 (1993).
[11] Y.S. Kim *et al.* (unpublished).
[12] P. Hofmann *et al.*, Phys. Rev. C **49**, 2555 (1994).
[13] A. Angelopoulos *et al.*, Phys. Lett. B **205**, 590 (1988).
[14] B. Chen *et al.*, Phys. Rev. C **45**, 2332 (1992).
[15] E.D. Minor, T.A. Armstrong, B. Chen, R.A. Lewis, and G.A. Smith, Z. Phys. A **342**, 447 (1992).
[16] D. Polster *et al.*, Phys. Lett. B **300**, 317 (1993).
[17] B. Van den Bossche and J. Vandermeulen, Z. Phys. A **348**, 281 (1994).
[18] I.A. Pshenichnov *et al.* (unpublished).
[19] R.A. Cecil, B.D. Anderson, and R. Madey, Nucl. Instrum. Methods **161**, 439 (1979).
[20] A.S. Iljinov, V.I. Nazaruk, and S.E. Chigrinov, Nucl. Phys. **A382**, 378 (1982).
[21] J. Cugnon and J. Vandermeulen, Ann. Phys. Fr. **14**, 49 (1989).
[22] H. Machner *et al.*, in *Proceedings of the Symposium on Nuclear Physics*, edited by D.R. Chakrabarty and Suresh Kumar (Bhaba Atomic Research Centre, Bombay, 1992), Vol. 35A, p. 65.
[23] E.D. Minor, T.A. Armstrong, R. Bishop, V. Harris, R.A. Lewis, and G.A. Smith, Z. Phys. A **336**, 461 (1990).
[24] V.V. Barmin *et al.*, Nucl. Phys. **A556**, 409 (1993).
[25] J. Riedelberger *et al.*, Phys. Rev. C **40**, 2717 (1989).
[26] D. Polster, D. Hilscher, H. Rossner, and H. Märten, Annual Report 1991, HMI, Berlin, 1992, p. 96.
[27] T.A. Armstrong, R. Bishop, V. Harris, R.A. Lewis, E.D. Minor, and G.A. Smith, Z. Phys. A **332**, 467 (1989).
[28] J. Cugnon and J. Vandermeulen, Nucl. Phys. **A445**, 717 (1985).
[29] P. Jasselette, J. Cugnon, and J. Vandermeulen, Nucl. Phys. **A484**, 542 (1988).
[30] E. Hernandez and E. Oset, Nucl. Phys. **A455**, 584 (1986).
[31] M. Hillman and Y. Eyal (unpublished); modified by H. Rossner.
[32] J. Cugnon, P. Jasselette, and J. Vandermeulen, Nucl. Phys. **A470**, 558 (1987).
[33] J.P. Bocquet *et al.*, Z. Phys. A **342**, 183 (1992).
[34] M.R. Clover, R.M. DeVries, N.J. DiGiacomo, and Y. Yariv, Phys. Rev. C **26**, 2138 (1982).
[35] D. Polster, Ph.D. thesis, Free University, 1994.
[36] W.M. Bugg, G.T. Condo, E.L. Hart, H.O. Cohn, and R.D. McCulloch, Phys. Rev. Lett. **31**, 475 (1973).
[37] J. Jastrzebski *et al.*, Nucl. Phys. **A558**, 405c (1993).
[38] J.D. Stevenson, Phys. Rev. Lett. **45**, 1773 (1980).
[39] Ye.S. Golubeva, A.S. Iljinov, A.S. Botvina, and N.M. Sobolevsky, Nucl. Phys. **A483**, 539 (1988).
[40] Ye.S. Golubeva, A.S. Iljinov, and I.A. Pshenichnov, Yad. Fiz. **57**, 1743 (1994) [J. At. Nucl. **57**, 1672 (1994)].
[41] A.A. Sibirtsev, Z. Phys. A **350**, 269 (1994).
[42] D. Polster, D. Hilscher, L. König, H. Rossner, and H. Märten, Annual Report 1991, HMI, Berlin, 1992, p. 79.
[43] G.F. Bertsch and S. Das Gupta, Phys. Rep. **160**, 189 (1988).
[44] B.A. Li, Nucl. Phys. **A556**, 147 (1993).
[45] B.A. Li (private communication).
[46] D. Hilscher, in *Proceedings of a Specialist Meeting on Preequilibrium Nuclear Reactions*, Semmering, Austria, 1988, edited by B. Strohmaier (OECD, Paris, 1988), p. 245.
[47] M. Farine, T. Sami, B. Remaud, and F. Sébille, Z. Phys. A **339**, 363 (1991).
[48] T. Maruyama, A. Ohnishi, and H. Horiuchi, Phys. Rev. C **45**, 2355 (1992).
[49] H.K.W. Leegte, A.L. Boonstra, J.D. Hinnefeld, E.E. Koldenhof, R.H. Siemssen, K. Siwek-Wilczyńka, Z. Sosin, J. Wilczyński, and H.W. Wilschut, Phys. Rev. C **46**, 991 (1992).
[50] A. Bohr and B.R. Mottelson, *Nuclear Structure* (Benjamin, New York, 1969), Vol. 1, p. 146.
[51] S. Teis, W. Cassing, T. Maruyama, and U. Mosel, Phys. Lett. B **319**, 47 (1993).
[52] P.J. Siemens and J.I. Kapusta, Phys. Rev. Lett. **43**, 1486 (1979).
[53] D.H.E. Gross, Z. Xiao-ze, and X. Shu-yan, Phys. Rev. Lett. **56**, 1544 (1986).
[54] D. Hilscher *et al.*, in *Proceedings of the LEAP '94 Conference*, Bled, Slovenia, 1994, edited by M. Mikuz (World Scientific, Singapore, 1995).

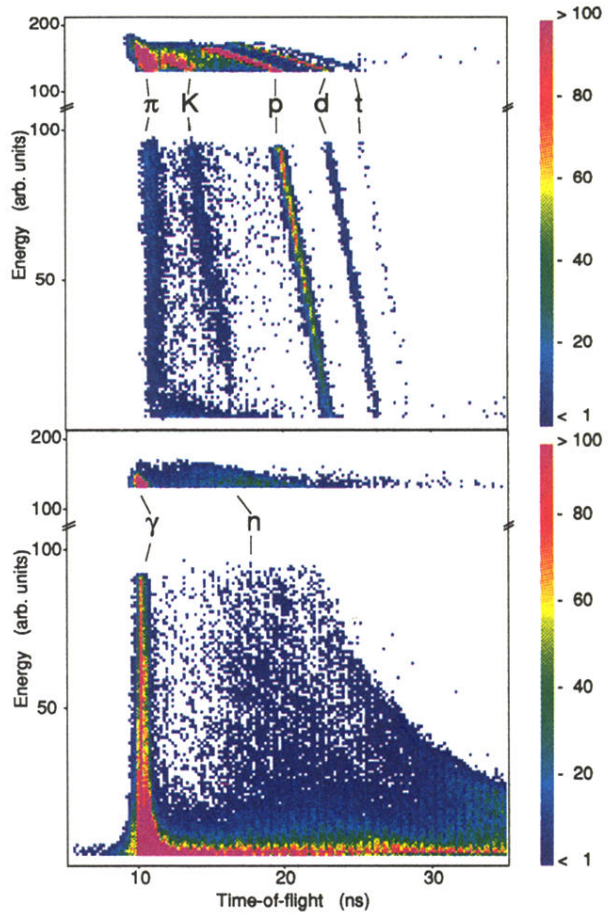

FIG. 3. The energy signal E (recoil energy for neutrons) of the liquid scintillator $N3$ as measured via the light output is plotted versus the time of flight: (a) with a coincidence requirement of the scintillator paddle in front of the liquid scintillator corresponding to charged particles ($\pi^{\pm}$,$K^{\pm}$, p, d, t) and (b) with an anticoincidence corresponding to neutrals (γ and n). The top part in each panel is the offset continuation of the lower part with a reduced energy gain by about a factor of 10.